15 October 1982, Volume 218, Number 4569 SCIENCE

Thermal-Wave Imaging

Allan Rosencwaig

In thermal-wave imaging, macroscopic and microscopic thermal features on or beneath the surface of a sample can be detected and imaged. This technique, although new, is an outgrowth of a much older methodology most commonly referred to as photoacoustics or photoacoustic spectroscopy (*1*). The photoacoustic effect, in which optical energy absorbed by a sample is detected through the subsequent thermal generation of acoustic signals, was discovered by Alexander Graham Bell more than 100 years ago (*2*). The discovery, however, found few scientific or technical applications and was soon consigned to the scientific footnotes of the 19th century. Only in recent years has it developed into a popular research and analytical tool in such diverse areas as chemistry, physics, biology, and medicine.

Summary. Thermal features on and beneath the surface of a sample can be detected and imaged with a thermal-wave microscope. Various methodologies for the excitation and detection of thermal waves are discussed, and several applications, primarily in microelectronics, are presented.

The photoacoustic effect is dependent not only on the sample's optical properties, but also on its thermal characteristics. Thus, some researchers have begun to investigate the photoacoustic effect as a probe of local variations in the thermal properties of samples. It is from these investigations that the field of thermal-wave imaging of a sample's thermal features has emerged. Thermal features can be defined as those regions of an otherwise homogeneous material that exhibit variations, relative to their surroundings, in any of the following three thermal parameters: density, ρ; specific heat, C; and, most important, thermal conductivity, κ. Variations in these thermal parameters arise, in the most general sense, from variations in the local lattice structure of the material.

If the original structure is highly ordered, as in the case of semiconductor crystals, then quite minor disruptions in the lattice structure can result in detectable thermal features. Examples of such minor disruptions result from the addition, by diffusion or implantation, of foreign ions in concentrations of less than $1:10^3$, or from the presence of vacancies or other lattice defects. These lattice disruptions have a measurable effect on the thermal conductivity, which, being a transport property, is highly sensitive to phonon scattering and thus to the degree of lattice disorder present. However, such minor lattice disruptions will generally have a negligible effect on the local optical and elastic parameters, which are essentially a measure of the statistical average of all the interatomic bonds. Thus thermal features arising from minor lattice disruptions will, in general, not be detectable with conventional optical or acoustic probes, but can be detected with the thermal-wave technique.

Other thermal features result from more substantial disruptions of the lattice network—such as those due to a change in the basic material composition or to the presence of mechanical defects such as cracks, voids, or delaminations. Many of these features can be imaged by optical, x-ray, or acoustic probes. Yet here, too, thermal-wave imaging offers some advantages. In opaque samples, for which x-ray or acoustic probes are now used, there are severe resolution limitations. Micrometer-sized features cannot be imaged with x-rays and can be imaged with acoustics only with complex ultrahigh frequency (1000 megahertz or greater) acoustic microscopes. Such features can be imaged with simpler thermal-wave microscopes operating at frequencies below 10 MHz. Also, thermal-wave imaging offers the opportunity for nondestructive depth-profiling, whereby the thermal features can be examined in three dimensions.

In summary, a thermal-wave probe is generally a much more sensitive detector of local variations in the lattice structure than are photon (optical or x-ray) or acoustic probes. In addition, the thermal-wave microscope often offers greater resolving capability than more conventional microscopes.

Imaging with Surface Temperature and Thermoacoustic Detectors

Figure 1 schematically depicts the basic physical processes that occur in a thermal-wave experiment. A beam of energy, usually a laser or electron beam, is focused and scanned across the surface of a sample. This beam is intensity-modulated at a frequency in the range 10 Hz to 10 MHz. As the beam scans across the sample it is absorbed at or near the surface, and periodic surface heating results at the beam modulation frequency. This periodic heating is the source of thermal waves, which propagate from the heated region. The thermal waves are diffusive waves similar to eddy current waves, evanescent waves, and other critically damped phenomena that travel only one to two wavelengths before their intensity becomes negligibly small. Nevertheless, within their range, the thermal waves interact with thermal features in a manner that is mathematically equivalent to the scattering and reflection processes of conventional propagating waves (*3*). Thus any features on or be-

The author is president of Therma-Wave, Inc., Fremont, California 94539.

neath the surface of the sample that are within the range of these thermal waves and that have thermal characteristics different from their surroundings will reflect and scatter the thermal waves and thus become visible.

Imaging of these thermal features requires detection of the scattered and reflected thermal waves. This detection is currently accomplished by several different techniques. As is often the case in a rapidly growing field, most discussions of these techniques have tended to emphasize their relative differences. It is more important, however, to stress their basic similarity—in particular, the fact that all of these techniques detect the scattered and reflected thermal waves through the effect of the thermal waves on either the local temperature on the surface of the sample or the thermoacoustic signal in the bulk of the sample.

As seen in Fig. 1, thermal waves scattered and reflected from the subsurface thermal feature alter the local surface temperature. Several methods have been developed to monitor variations in this parameter. The earliest was scanning photoacoustic microscopy (SPAM) (*4–7*), in which gas-microphone photoacoustics is used to monitor the variations in local surface temperature. The surface temperature oscillations produce variations in the gas pressure inside a closed photoacoustic cell as a result of the periodic conduction of heat from the sample surface to the gas in the cell. Another technique, photothermal imaging (*8–10*), involves detection of the infrared radiation emitted from the periodically heated spot on the sample. A third technique—referred to as the mirage effect (*11*) or as optical beam deflection (OBD) (*12*)—is based on periodic heat conduction from the heated spot on the sample surface to the local layer of gas or liquid adjacent to it. This technique measures the deflection of a laser beam traversing the periodically heated gaseous or liquid layer. All these techniques detect the thermal waves that are scattered and reflected from local thermal features through the effect of these waves on the surface temperature. However, all these surface temperature monitoring methods are impractical at frequencies exceeding 10 kHz and thus are severely limited in imaging resolution.

Table 1. Thermal-wave spatial resolution for thermal conductors (silicon, metals) and thermal insulators (oxides, biological materials).

Modulation frequency	Thermal conductor	Thermal insulator
100 Hz	200 to 300 μm	20 to 30 μm
10 kHz	20 to 30 μm	2 to 3 μm
1 MHz	2 to 3 μm	2000 to 3000 angstroms

The resolution obtainable in thermal-wave imaging is set by both the spot size of the incident energy beam and the thermal wavelength. The thermal wavelength is given by

$$\lambda_{th} = 2\pi\left(\frac{2\kappa}{\rho C\omega}\right)^{1/2} \tag{1}$$

where ω is the angular frequency at which the beam is modulated. One can show that the thermal-wave resolution is limited to $\sim \lambda_{th}/2\pi$. As seen in Table 1, thermal resolution for thermal conductors at 10 kHz is only 20 to 30 μm, and micrometer-range resolution requires beam modulation frequencies of 1 MHz or greater, which are not practical for the surface temperature detection techniques described above.

To overcome this resolution limitation, Rosencwaig (*13, 14*) suggested that the scattered and reflected thermal waves can be detected through their effect on the thermoacoustic signals generated in the bulk of the sample. Such signals can be detected at high frequencies by using ultrasonic transducers in acoustic contact with the sample. He also suggested that various means, including electron as well as laser beams, could be used to excite the thermal waves. The first thermal-wave experiments based on the thermoacoustic probe concept were performed with a laser beam (*15, 16*), and subsequent experiments were performed with an electron beam (*17, 18*) in a conventional scanning electron microscope. Since then, many other examples of thermal-wave imaging with scanning electron microscopes have been reported (*19, 20*).

Thermoacoustic signals occur in any sample with a nonzero thermal expansion coefficient because of the periodic stress-strain conditions in the heated volume defined by the thermal waves. Thus, as depicted in Fig. 1, the 1-MHz thermal waves give rise to 1-MHz acoustic waves. These thermoacoustic waves are propagating waves of much longer wavelengths—typically a few millimeters at 1 MHz compared to a few micrometers for thermal waves at the same frequency. The magnitude and phase of the thermoacoustic waves are directly related to the temperature profiles in the heated volume and thus are directly affected by the presence of scattered and reflected thermal waves.

Thermoacoustically generated ultrasonic waves were predicted by White (*21*) and first used for imaging by von Gutfeld and Melcher (*22*). These and subsequent experiments were concerned, however, with the use of thermoacoustic waves for ultrasonic imaging, where the interactions of the acoustic waves with the elastic features in the sample produce the principal image features. The possibility of using the thermal waves, which precede the thermoacoustic waves, for the imaging of thermal features was not realized at that time. Although acoustic waves are detected, thermal-wave imaging with the thermoacoustic probe is not acoustic imaging, since the acoustic waves always have wavelengths many orders of magnitude greater than the thermal waves and thus are not able to image the same small features. That is, the acoustic waves simply carry or amplify the information

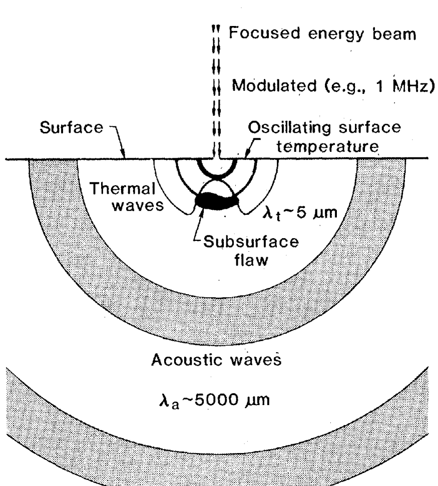

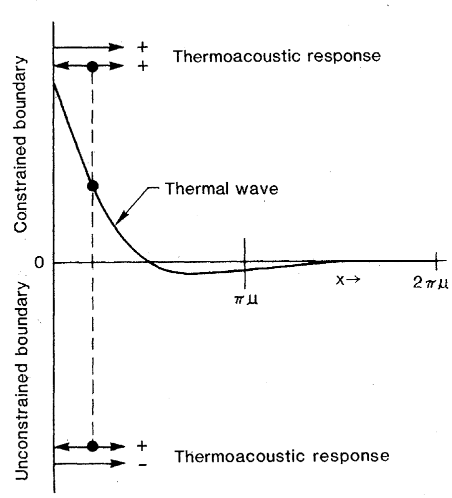

Fig. 1 (left). Schematic representation of the physical processes that occur during thermal-wave imaging. Fig. 2 (right). Schematic representation of the relation between thermal and thermoacoustic waves. Thermoacoustic wavelengths are much larger than thermal wavelengths and thus strong constructive or destructive thermoacoustic interference occurs if the heated surface is constrained or free, respectively.

describing the thermal-wave event. In thermal-wave imaging, the thermoacoustic waves are thus used as a monitor to detect the presence of thermal waves scattered or reflected from thermal features, just as infrared emission is used as a surface temperature probe of scattered and reflected thermal waves.

Although both the surface temperature and the thermoacoustic probes can be used to detect thermal waves, none of these detection techniques is a perfectly clean monitor of thermal waves, for each is also sensitive to at least one other locally varying sample parameter. For example, SPAM is sensitive to local surface conditions or morphology affecting heat conduction to the gas. The photothermal technique is sensitive to local changes in the infrared emissivity of the surface, and the mirage or OBD method is sensitive to both local heat conduction variations and surface topology. Similarly, the thermoacoustic probe is sensitive to variations in the thermal expansion coefficient and the elastic constants within the thermal diffusion volume of the sample. However, to dwell on these differences is to ignore the unique capability of all of these methods for thermal-wave imaging. To illustrate this, consider a sample such as a polished silicon wafer lightly doped with a pattern of implanted or diffused ions. Such a sample will have no variations in surface morphology, topology, or emissivity and no measurable variations in local thermal expansivity or elastic parameters. It will thus exhibit only thermal features, and all of the techniques described above, if operated at the same beam modulation frequency, will produce the same thermal-wave image of the sample.

Theory

No technology can be truly useful without a good theoretical model. Although several very good theories have been developed that can be applied to thermal-wave imaging (*3, 9, 23–27*), these theories have all been particularized for specific detector methodologies. A more general theoretical model, developed recently by Opsal and Rosencwaig (*28*), is applicable to thermal-wave imaging performed with either a surface temperature probe or a thermoacoustic probe. Although one-dimensional, this theory provides an adequate representation of the basic physical processes that occur during thermal-wave imaging.

The Opsal-Rosencwaig theory shows that a surface temperature probe will always provide information about a thermal feature as long as the feature is within the range of the thermal waves. However, the utility of the thermoacoustic probe for thermal-wave imaging depends on the elastic conditions at the sample surface. As predicted by White (*21*) and subsequently verified by von Gutfeld and Melcher (*22*), a mechanically constrained surface provides stronger thermoacoustic signals and thus is the preferred arrangement for ultrasonic imaging with thermoacoustic waves. Recently, Wetsel (*29*) reported that mechanical constraint with an overlay material of suitable thermal and elastic properties can further enhance this effect. However, Opsal and Rosencwaig have shown that such mechanically constrained surfaces produce thermoacoustic signals that provide no data on thermal features. Instead, it is the weaker thermoacoustic signal obtained from a mechanically free surface that provides data on the thermal features.

To illustrate this point, Fig. 2 shows a typical one-dimensional thermal wave generated by periodic heating of the sample surface. The thermoacoustic response arises from the local thermal expansion occurring at every point along the thermal wave. The response is basically a weighted average of the temperatures throughout the material, where the weight factor is the thermoacoustic response to a source of unit strength. In all applications of practical interest, the acoustic wavelength is much larger than the thermal wavelength, and the thermoacoustic response can be represented by a rapidly converging series in which only the first two terms are significant.

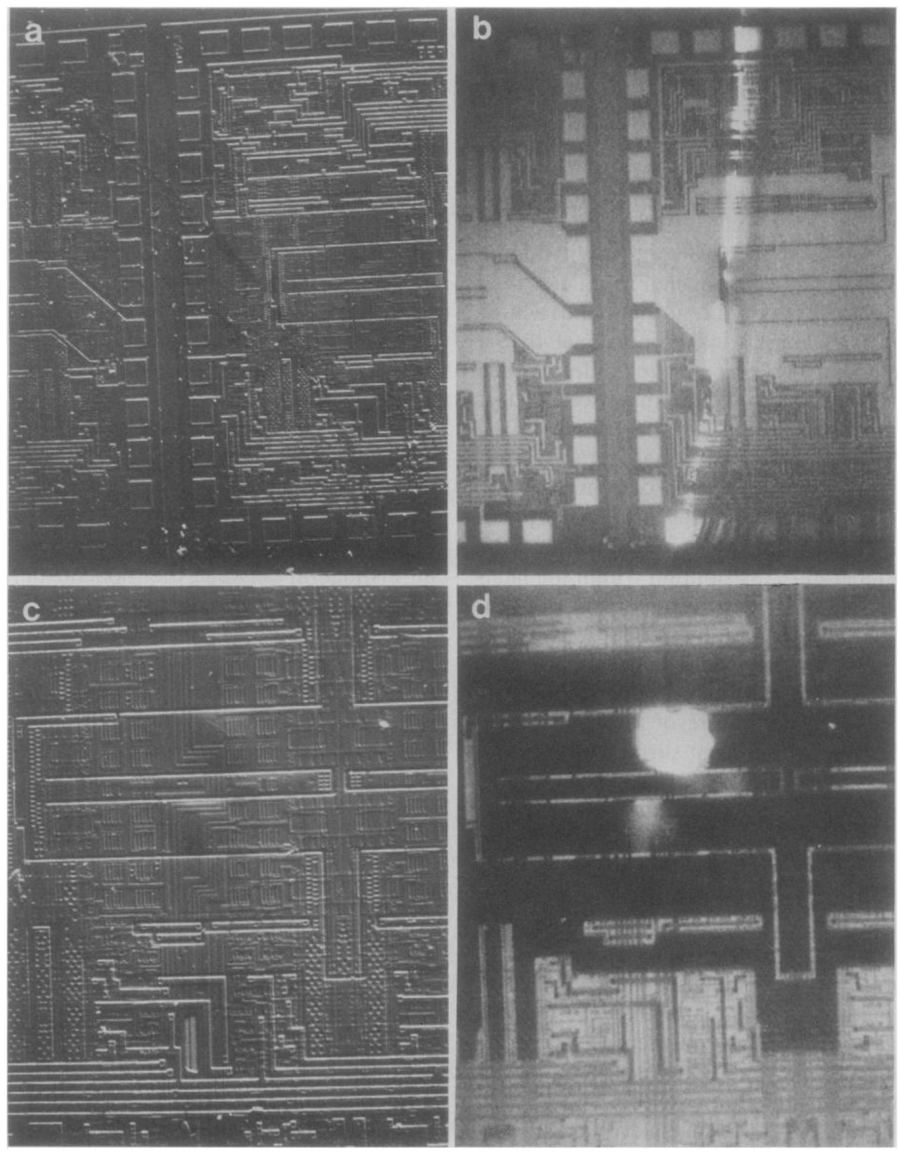

Fig. 3. Examples of subsurface mechanical defects in silicon integrated circuits: (a and c) backscattered-electron images exhibiting no visible signs of defects; (b and d) thermal-wave images of the same areas, showing (b) a subsurface microcrack and (d) local subsurface delaminations (irregular white regions in upper center).

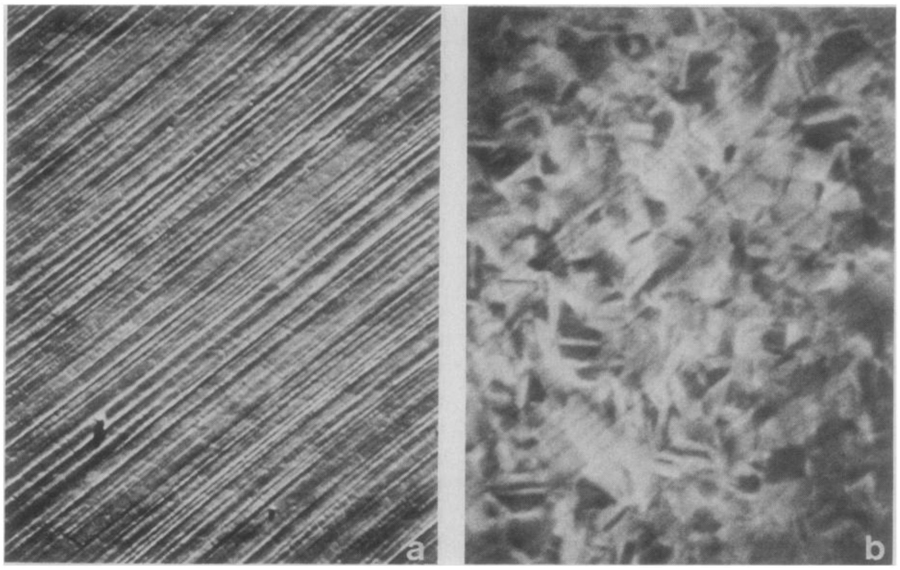

Fig. 4. Images of a 309S stainless steel alloy: (a) backscattered-electron image showing machining marks; (b) thermal-wave image showing, in addition, face-centered cubic austenitic grains and annealing twins.

The first term is simply proportional to the temperature averaged over the heated volume and therefore is very insensitive to the presence of local thermal features, particularly those arising from variations in thermal conductivity alone. The second term, which is smaller than the first by the ratio of thermal to acoustic wavelengths, is proportional to the average of temperature differentiated with respect to the thermal wave vector. This term is thus quite sensitive to the presence of local thermal features. Stated differently, the first two terms in the thermoacoustic series are proportional to the zeroth and first moments of the temperature distribution within the heated volume. The zeroth moment is insensitive and the first moment is sensitive to the presence of local thermal features.

The thermoacoustic response also depends on the nature of the acoustic reflections at the front surface of the sample. As seen in Fig. 2, two elastic waves emanate from any point on the thermal wave, one going to the right, the other to the left. For a mechanically constrained or rigid surface, the left-going wave undergoes no change of phase and thus interferes constructively with the right-going wave. Since the acoustic wavelength is much greater than the thermal wavelength, this interference is quite strong, and thus the thermoacoustic response is dominated by the first term in the series. A mechanically constrained surface therefore results in a large thermoacoustic signal, but one that is very insensitive to the presence of local thermal features. On the other hand, a mechanically free surface results in a 180° phase shift upon reflection of the left-going wave. Consequently, there is strong destructive interference with the right-going wave, and now the second term in the series dominates the thermoacoustic response. A mechanically free surface therefore results in a much weaker thermoacoustic signal, but one that is sensitive to the presence of local thermal features. Thus the sample configuration best suited for thermal-wave imaging with the thermoacoustic probe is the one least suited for ultrasonic imaging with thermoacoustic waves.

This theory illustrates another important distinction between thermoacoustic ultrasonic and thermal-wave imaging. The resolution in ultrasonic imaging depends not only on the wavelength of the acoustic waves, but also on the depth of penetration and the spreading of the incident beam beneath the surface. In the case of thermal-wave imaging, the resolution is dependent on the thermal wavelength and the beam spot size on the surface. In addition, only the beam spreading occurring within a thermal wavelength of the surface will affect the resolution. This is fairly obvious for the case of thermal-wave imaging with surface temperature monitoring. Although it is not as obvious, the same applies to the case of thermal-wave imaging with the thermoacoustic probe. The thermal-wave imaging depth must always be within a thermal wavelength of the surface, and the resolution of a thermal-wave image is not degraded by any beam spreading that occurs beyond this depth.

Applications of Thermal-Wave Imaging

Thermal waves are critically damped waves having a relatively short range. Thermal-wave imaging is thus near-surface, high-resolution imaging. Not surprisingly, therefore, most of the applications of thermal-wave imaging have been in microelectronics, where most of the features of interest lie within 10 μm of the surface. Nevertheless, there are important potential applications that remain to be explored in the areas of metallography, materials analysis, and biological investigations.

Some examples of high-resolution thermal-wave imaging performed with a thermoacoustic probe are presented here. The applications are divided into two main categories, corresponding to thermal features arising from significant changes in the sample's lattice structure and those arising from minor changes in the structure. Although in all of these examples a scanning electron microscope was used, a laser beam or other form of local thermal excitation could have been used as well.

Significant lattice changes. Examples of significant alterations of the lattice are changes in the basic material or in the chemical composition of the material, as might occur in a multilayer or heterogeneous sample. Other examples are mechanical defects such as voids, cracks, and delaminations. A thermal-wave image of such features is shown in Fig. 3. This image was taken with a scanning electron microscope equipped with a Therma-Wave, Inc., thermal-wave imaging system. Figure 3a shows the backscattered-electron image of a silicon integrated circuit with no visible sign of defects. Figure 3b is the thermal-wave image of the same region and clearly shows a subsurface microcrack running vertically down the right-hand side of the imaged area. From the imaging range of the thermal waves, we know that this microcrack lies within 10 μm of the surface. Again, in Fig. 3c the backscattered-electron image of another silicon circuit shows no obvious defects. The thermal-wave image in Fig. 3d, however, shows the presence of local film delaminations (irregular white regions in upper central area), which appear to be the results of subsurface "blistering." As with the microcrack, these delaminations lie within 10 μm of the surface.

Another example of significant lattice variations occurs in materials that exhibit several phase structures. Figure 4 shows the backscattered-electron and thermal-wave images of a 309S stainless steel alloy. The electron image is dominated by rough machining marks on the surface and gives little indication of any other features. The thermal-wave image shows the machining marks but also clearly shows various face-centered cubic grains in this austenitic steel, including the presence of annealing twins. Such crystalline grains can be seen with conventional optical or electron microscopy only after special sample preparation. Other interesting examples of thermal-wave imaging in crystallographically heterogeneous materials have been reported by Cargill (*20*).

Minor lattice changes. Significant lattice changes, such as those in the examples above, result in measurable variations not only in local thermal properties but also in local optical and elastic properties. Thus these features can, in principle, also be imaged with x-rays or with an ultrasonic or acoustic microscope. When the changes in the lattice structure are relatively minor, the effect on optical and elastic parameters is undetectable. However, if the lattice is initially highly ordered, then such minor changes can still produce measurable changes in the local thermal conductivity and can be imaged with a thermal-wave microscope.

An example of this capability is shown in Fig. 5 (*30*). The sample here is a silicon wafer that was first coated with 0.4 μm of oxide. A resolution pattern was photolithographed and etched into the oxide, and phosphorus was then thermally diffused into the patterned regions at a concentration of $\sim 10^{19}$ molecules per cubic centimeter. After the doping, the oxide was stripped from most of the wafer. In the backscattered-electron image (Fig. 5a), the patterned regions are visible only along the far right edge of the wafer, where the oxide is still present. No patterns are visible in the bare silicon region, even though patterned dopant regions are present here. Only in the thermal-wave image of this region (Fig. 5b) is all of the resolution pattern visible, both the portion etched in the oxide and that present only as phosphorus-doped regions in the bare silicon. Similar results have been obtained with various ion-implanted dopants and detection sensitivities as low as 1×10^{11} cm^{-2} have been obtained with arsenic implantation.

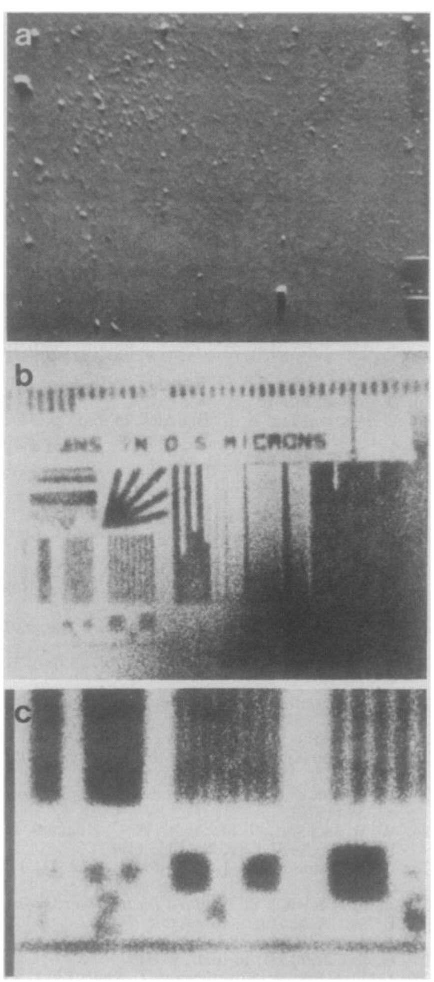

Fig. 5. Images of a phosphorus-doped silicon wafer: (a) backscattered-electron micrograph showing a resolution pattern only at the far right, where oxide is still present; (b) thermal-wave image showing the full resolution pattern; (c) magnified thermal-wave image showing the resolution of the phosphorus-doped silicon pattern in bare silicon to be ~ 3 μm at a modulation frequency of 1 MHz.

Another interesting example of thermal-wave detection of lattice perturbations is shown in Fig. 6. A sample of GaAs was first masked in a pattern and then bombarded with energetic protons (40 kiloelectron volts) at a flux of 10^{15} per square centimeter (*31*). These protons produced a controlled defect zone of vacancies and interstitials about 0.5 μm below the surface wherever the GaAs was not protected by the mask. The backscattered-electron image of the GaAs, after removal of the mask, shows no visible patterns (Fig. 6a). However, the thermal-wave image of the same area (Fig. 6b) clearly shows the masking pattern (white regions). The image contrast arises from the fact that the proton-bombarded GaAs (dark regions) now has a lower thermal conductivity than the unperturbed GaAs. In fact, even the masked-off regions are somewhat perturbed, since closer examination of the thermal-wave image shows several areas where there has apparently been proton penetration through defects in the mask.

By using a 1-MHz beam modulation frequency, we have obtained a thermal-wave resolution in silicon of ~ 3 μm. Because GaAs has a lower thermal conductivity and a greater density, the thermal wavelength, as given by Eq. 1, is significantly lower in GaAs and thus our resolution is close to 1 μm in this semiconductor material for 1-MHz beam modulation. Figure 6, b and c, illustrates this increased resolution with images of 2-μm crosslines in the proton-bombarded pattern.

Nondestructive depth-profiling. A unique feature of thermal-wave imaging is the ability to obtain images from different depths beneath the surface. The total penetration depth of the thermal waves can be changed by varying the thermal wavelength through the modulation frequency. Also, the depth within the penetration range from which the primary

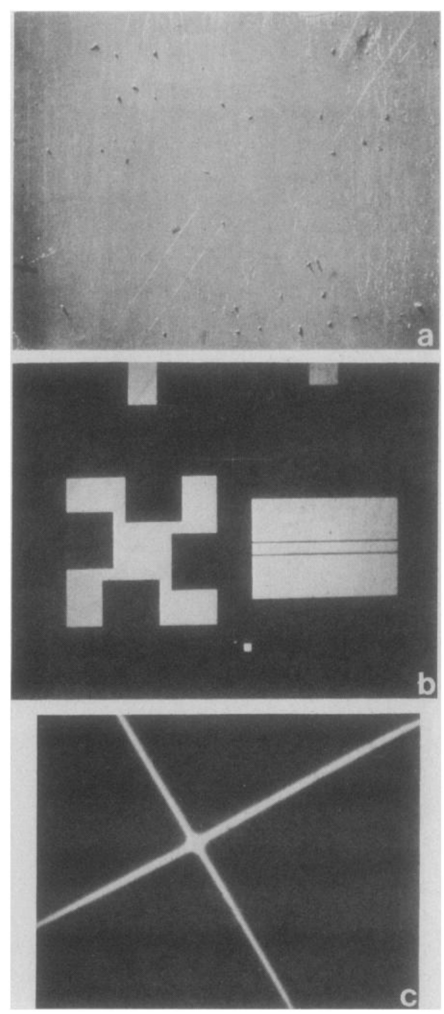

Fig. 6. Images of a proton-bombarded GaAs wafer: (a) backscattered-electron micrograph of the GaAs sample after removal of the mask, showing no evidence of the masking pattern; (b) thermal-wave image of same region showing proton-bombarded (dark) regions and unperturbed (white) regions; (c) magnified thermal-wave image of 2-μm lines in a proton-bombarded region, indicating a thermal-wave resolution in GaAs of ~ 1 μm at 1 MHz.

image comes can be set by changing the phase of detection (*32*). This is a result of the critically damped nature of the thermal waves. A change of phase of 90° can change the image depth from close to the surface (one-tenth of the penetration depth) to considerably deeper (one-third of the total penetration depth).

Figure 7 is an example of nondestructive depth-profiling. The backscattered-electron image (Fig. 7a) shows a region of silicon circuit bounded by two metal pads. The thermal-wave image in Fig. 7b was obtained at a frequency and phase setting such that the major part of the image is from ~ 1 μm beneath the surface. In Fig. 7c the phase has been changed and the image is from ~ 3 μm beneath the surface; the differences from Fig. 7b are most likely due to changes of either material composition or doping levels in the silicon as a function of depth beneath the surface.

Conclusions

Thermal-wave imaging is a means of detecting and imaging previously invisible thermal features. Its applications in the field of microelectronics are many and diverse. They include the detection and imaging of subsurface defects, including interfacial flaws and microcracks; detection and characterization of areas of the semiconductor lattice that have been modified through the introduction of foreign ions or defects; and the use of depth-profiling to obtain quantitative measurements of thin-film thickness and of dopant depth profiles.

The potential applications in other fields are equally exciting. The ability to image crystalline phases and grains in alloys and heterogeneous materials with no special sample preparation makes possible more convenient, in situ, and perhaps even dynamic studies of metals, composites, and other materials. In biology the method may be used to analyze and map the microscopic structure of membranes and cells in terms of their thermal parameters, and may well produce valuable new results.

Finally, I emphasize again that the concept of thermal-wave imaging transcends any particular methodology for the generation and detection of the thermal waves. Any intensity-modulated beam of energy, whether it is an electron beam or is from a laser or any other source, can be used to excite thermal waves. Similarly, any of several methods—based on one of the surface temperature probes or on a thermoacoustic probe—can be used to detect the thermal waves. To fully appreciate the potential of thermal-wave imaging, one must look beyond the details of the particular excitation and detection methodologies and understand the basic principles of the method.

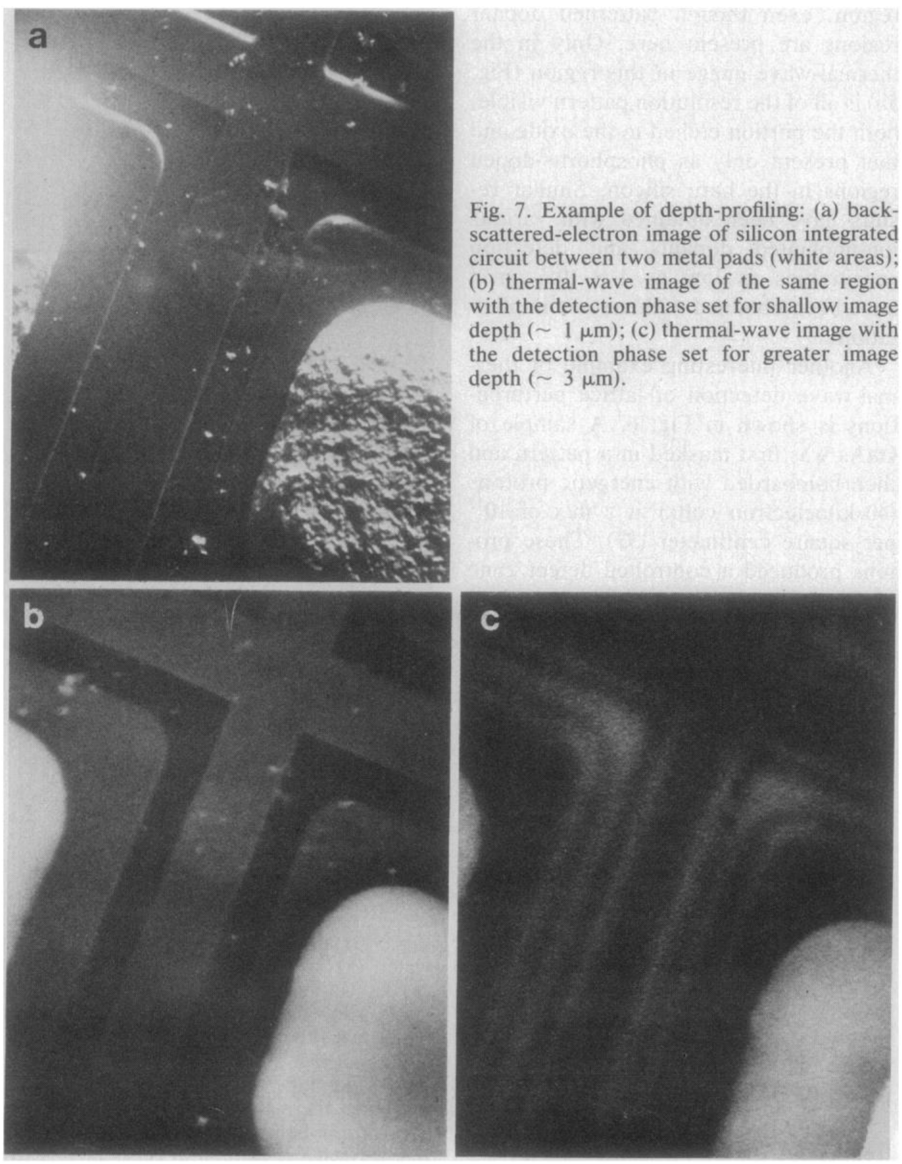

Fig. 7. Example of depth-profiling: (a) backscattered-electron image of silicon integrated circuit between two metal pads (white areas); (b) thermal-wave image of the same region with the detection phase set for shallow image depth (~ 1 μm); (c) thermal-wave image with the detection phase set for greater image depth (~ 3 μm).

References and Notes

1. A. Rosencwaig, *Photoacoustics and Photoacoustic Spectroscopy* (Wiley, New York, 1980).
2. A. G. Bell, *Philos. Mag.* **11** (No. 5), 510 (1881).
3. R. L. Thomas *et al.*, *J. Appl. Phys.* **51**, 1152 (1980).
4. Y. H. Wong, R. L. Thomas, G. F. Hawkins, *Appl. Phys. Lett.* **32**, 538 (1978).
5. Y. H. Wong, in *Scanned Image Microscopy*, E. A. Ash, Ed. (Academic Press, London, 1980), p. 247.
6. M. Luukkala and A. Penttinen, *Electron. Lett.* **15**, 325 (1979).
7. G. Busse, *Appl. Phys. Lett.* **35**, 759 (1979).
8. M. Luukkala, in *Scanned Image Microscopy*, E. A. Ash, Ed. (Academic Press, London, 1980), p. 273.
9. P.-E. Nordal and S. O. Kanstad, in *ibid.*, p. 331.
10. G. Busse, in *ibid.*, p. 341.
11. D. Fournier and A. C. Boccara, in *ibid.*, p. 347.
12. J. C. Murphy and L. C. Aamodt, *Appl. Phys. Lett.* **38**, 196 (1981).
13. A. Rosencwaig, U.S. Patent 4,255,971, 17 March 1981.
14. ———, *Am. Lab.* **11** (No. 4), 39 (1979).
15. G. Busse and A. Rosencwaig, *Appl. Phys. Lett.* **36**, 815 (1980).
16. A. Rosencwaig and G. Busse, *ibid.*, p. 725.
17. E. Brandis and A. Rosencwaig, *ibid.* **37**, 98 (1980).
18. G. S. Cargill III, *Nature (London)* **286**, 691 (1980).
19. A. Rosencwaig, *Solid State Technol.* **25** (No. 3), 91 (1982).
20. G. S. Cargill III, *Phys. Today* **34**, 27 (October 1981).
21. R. M. White, *J. Appl. Phys.* **34**, 559 (1963).
22. R. J. von Gutfeld and R. L. Melcher, *Appl. Phys. Lett.* **33**, 257 (1977).
23. A. Rosencwaig and A. Gersho, *J. Appl. Phys.* **47**, 64 (1976).
24. W. B. Jackson, N. M. Amer, A. C. Boccara, D. Fournier, *Appl. Opt.* **20**, 1333 (1981).
25. L. C. Aamodt and J. C. Murphy, *ibid.* **21**, 111 (1982).
26. A. Rosencwaig, in *Scanned Image Microscopy*, E. A. Ash, Ed. (Academic Press, London, 1980), p. 300.
27. G. S. Cargill III, in *ibid.*, p. 319.
28. J. Opsal and A. Rosencwaig, *J. Appl. Phys.* **53**, 4240 (1982).
29. G. C. Wetsel, Jr., in *Proceedings of the 1980 Ultrasonics Symposium*, B. R. McAvoy, Ed. (IEEE Press, New York, 1980), p. 645.
30. A. Rosencwaig and R. M. White, *Appl. Phys. Lett.* **38**, 165 (1981).
31. The GaAs sample was kindly provided by T. Kirkendall COMSAT Laboratories, Clarksburg, Maryland.
32. A. Rosencwaig, *Electron. Lett.* **16**, 928 (1980).